Topics in Catalysis
https://doi.org/10.1007/s11244-024-02014-7

ORIGINAL PAPER

Simultaneous Electrochemical Detection of Paraquat and Carbofuran Using a Biodegradable Flexible Electrode, Enhanced with Carbon Nitride Dots and Poly(allylamine hydrochloride) via Layer-by-Layer Technique

Amanda de S. M. de Freitas[1] · Lucas V. B. V. Fré[1] · Jéssica S. Rodrigues[2] · Stefanny F. Amaro[1] · Anerise de Barros[3] · Maria E. S. Nascimento[1] · Marystela Ferreira[1]

Accepted: 10 September 2024

Abstract
The developing of sensor devices for portable and selective detection remains an emergent technology needed for monitoring water contamination. In this work, we developed a flexible and biodegradable sensor based on the polymer poly(butylene adipate-co-terephthalate) (PBAT) mixed with graphite (g), creating (g-PBAT) for the simultaneous detection of paraquat (PQ) and carbofuran (CBF) pesticides. The g-PBAT was used as an electrode support and was modified with poly(allylamine hydrochloride) and carbon nitride dotes by Layer-by-Layer technique. The sensor's performance was evaluated through electrochemical methods using cyclic voltammetry, electrochemical impedance spectroscopy, and differential pulse voltammetry. The results demonstrated good reproducibility and repeatability with RSD of 14% and 8.8%, respectively. The stability in terms of current signal peak increased by only 8.5% compared to the initial cycle. The limit of detection (LoD) and limit of quantification (LoQ) were 0.63 µM and 2.10 µM for PQ, respectively, with a sensitivity of 3.69E-5 ± 5.94E-7 A cm^{-2} M^{-1}, while the CBF had a LoD and LoQ of 7.14 µM and 23.8 µM, respectively, with a sensitivity of 2.51E-7 ± 2.09E-8 A cm^{-2} M^{-1}. Additionally, the recovery methodology for the real sample showed ranges from 89.3% to 105.0% for PQ, and 92.1% to 105.9% for CBF, indicating that the sensor exhibits good sensitivity and stable RSD, ranging from 4% to 7.5%.

Keywords Biodegradable sensor · Layer-by-layer · Carbon nitride dots · Paraquat and carbofuran

1 Introduction

Electrochemical sensing in agriculture holds significant promise, as this activity is crucial for sustaining humanity. It enhances production yields and prevents losses during cultivation, with is increasingly important given the growing world population. Advances in technology have expanded the variety and use of artificial fertilizers, pesticides, and the availability of essential resources like water and nutrients for plants [1]. As a result, electrochemical sensors have emerged as a viable strategy for detecting agricultural pesticides, such as paraquat (1,10-dimethyl-4,40-bipyridinium) (PQ), hydroquinone, carbofuran and many others [2–4]. Specifically, PQ is an herbicide used for weed control in agriculture, representing a significant risk to humans and animals due to its extreme toxicity. Moreover, exposure to PQ can cause eye irritation, skin and nail ulceration, and

Amanda de S. M. de Freitas, Lucas V. B. V. Fré and Jéssica S. Rodrigues have equally contributed to the manuscript.

✉ Marystela Ferreira
marystela@ufscar.br

[1] Science and Technology Center for Sustainability (CCTS), Federal University of São Carlos (UFSCar), Sorocaba, SP, Brazil

[2] Institute of Science and Technology (ICT), São Paulo State University (UNESP), Sorocaba, SP, Brazil

[3] Institute of Chemistry (IQ), State University of Campinas, Campinas, (UNICAMP)SP, Brazil

Published online: 14 October 2024

organ failure due to absorption by the liver, kidneys, and lungs [5, 6]. Another pesticide widely used as an insecticide, nematicide, and acaricide in agriculture, forestry, and gardening is carbofuran (N-methyl carbamate) (CBF). Exposure to or ingesting of CBF causes high morbidity and mortality in humans and pets. However, the inappropriate use of CBF causes it to accumulate in soil and water, polluting the environment and posing risks to human health. Therefore, developing new technologies to detect and monitor both (PQ and CBF) contaminants is extremely important to minimize damage [7, 8].

Polymeric materials have aroused great interest as a sensor platform, mainly due to their variety of features, including flexibility, mechanical resistance, and low cost [9]. Moreover, the incorporation of conductive materials such as graphite, carbon dots, and graphene, among others, into the polymeric matrix can enhance sensors' sensitivity and lower detection limits, acting as a transducer interface that exhibits features of electron acceptors and donors for electrochemical sensors [10]. The development of substrates that combine the use of polymer with graphite has already been described in the literature [3, 11, 12]. However, this study stands out because, besides describing the preparation of a biodegradable and flexible substrate, the LbL film [3, 5] used in functionalization is also environmentally friendly.

The fundamental principles of green chemistry have significantly influenced the evolution of analytical chemistry, emphasizing the importance of delivering accurate, high-quality information while minimizing environmental impact and reducing resource consumption. Green analytical chemistry prioritizes the use of safe, sustainable, and eco-friendly materials, as well as energy-efficient processes. Within this context, the electrode employed in this work exemplifies these principles, as it is straightforward to construct, requires minimal materials for surface modification, and aligns with the goals of sustainability. Its application is highly promising for environmental applications, particularly in the detection of harmful emissions, where green approaches are essential for protecting ecosystems and ensuring a sustainable future [13].

Surface modifications, also known as functionalization, of conductive polymeric substrates can be performed using a wide range of methodologies. Functionalization with self-assembled nanometric films using the LbL technique has been described as an efficient surface modification method. This approach makes the device more attractive, by allowing a greater surface area and improving electrolytic activity, with deposition that is independent of the nature, size, and topology [14, 15]. The film used for the modification is composed of CND, a material that has gained prominence due to its photophysical and structural properties, combined with its solubility in water and synthesis with precursors considered green. This differentiates CNDs from other commonly used carbon materials, such as carbon nanotubes, for example. It is also worth highlighting the combined use of PAH, a water-soluble and biodegradable cationic polyelectrolyte. The combined use of these materials allows the preparation of a film without the use of organic solvents and with minimal environmental impact.

This work aimed to produce and functionalize low-cost sensors that are environmentally friendly and can be reprocessed. The sensors produced were used to simultaneously detect PQ and CBF. The characterization of the obtained device was carried out using Fourier transform infrared (FTIR), Raman and ultraviolet–visible (UV–vis) spectroscopy, Scanning Electron Microscopy (SEM), and contact angle measurements. The electrochemical characterization techniques used were CV and EIS. The sensory activity in the detection of PQ and CBF was carried out using the DPV technique.

2 Materials and Methods

2.1 Materials

The materials used to fabricate a flexible sensor support and surface modification were the poly(butylene adipate-co-terephthalate) (PBAT), BASF, synthetic graphite powder (< 20 µm, assay 99%) and poly(allylamine hydrochloride) (PAH) purchased from Sigma-Aldrich. Hydrochloric acid (HCl) purchased from Synth. Paraquat (PQ) and carbofuran (CBF) analyte were purchased from Sigma-Aldrich, and the interfering species hydroquinone and methyl parathion were purchased by Vetec and Sigma-Aldrich, respectively. For electrochemical measurements, were used potassium chloride (KCl), potassium ferricyanide ($K_3[Fe(CN)_6]$), potassium phosphate dibasic (K_2HPO_4), potassium phosphate monobasic (KH_2PO_4) were purchased from Sigma-Aldrich. The solutions used in this work were all prepared with ultrapure water (Sartorius Weighing Technology, Göttingen, Germany) with resistivity of 18.2 MΩ cm at 25 °C.

2.2 CND Synthesis

CNDs were synthesized according to the procedure described by Maciel et al. [16]. Briefly, 0.5 g of citric acid and urea were measured and transferred to a glass bottle with 25 mL of water. This mixture was stirred vigorously for 24 h, then heated in the microwave at 700 W for 5 min. Afterward, the solid obtained was washed, centrifuged, and filtered with a 0.2 µm filter. The resulting material was dried in an oven at 90 °C, then characterized by fluorescence, and Raman spectroscopy analysis was carried out.

2.3 Study of Bilayer Growth with the Layer-by-Layer (LbL) Technique

Ultraviolet Visible spectroscopy analyses were performed using a Thermo Scientific Genesys 10 model UV–Vis spectrometer, in a wavelength range of 190 to 800 nm. The PAH and CND solutions prepared for use in the LbL technique were analyzed. Additionally, a study of bilayer growth was also carried out on a quartz substrate.

2.4 Modification of the g-PBAT Sensor by Layer-by-Layer

The g-PBAT substrate was produced by mixing graphite and PBAT in 70:30 ratio in 10 mL chloroform and finalized by evaporating solvent. The modification was carried out by constructing a nanostructured film using the LbL technique, as schematically shown in Fig. 1. To assemble the film, the substrate was immersed in an acidic PAH solution (pH 3.0) with a concentration of 1 mg/mL, for 10 min, followed by washing in an aqueous HCl solution (pH 3.0) for 30 s. Subsequently, the substrate was immersed in an aqueous solution of CND with a concentration of 1 mg/mL for 10 min, and then underwent a subsequent washing step in milli-Q water for 30 s. Thus, 5 bilayers were prepared (g-PBAT(CND/PAH)$_5$).

2.5 Physical Characterizations

The characterizations were carried out for g-PBAT and g-PBAT(CND/PAH)$_5$ samples, aiming to highlight the changes that occurred in the substrate after covering with the film. The sessile drop technique was performed using a Ramé Hart goniometer (model 100-00) with deionized water. In this method, 3 drops of water at different points on the surface, each resulting in 10 contact angle measurements. The results represent an average of 30 measurements. A morphological characterization study was performed using a SEM, model FEI Quanta 250 FEG (FEI Co., Hillsboro, OR, USA), with an acceleration of 2 kV and tungsten filament. Subsequently, the samples were covered with a thin iridium film using a metallizer model MED020 Baltec. Using a Nicolet Summit IR 200 FT-IR model, structural characterization of the films was in reflectance mode, using 126 scans with nominal resolution of 4.0 cm^{-1}, in a range of 4000 to 400 cm^{-1}. Raman analyses were performed on a HORIBA Jobin Yvon T64000 Raman spectrometer coupled with an Olympus BX41 microscope, measurements were performed with incident excitation radiation at a wavelength 633 from a Research electro-Optics with a 10% filter, 20 s of exposure, 1 accumulation, on an 1800 gr/mm grating and 10× objective.

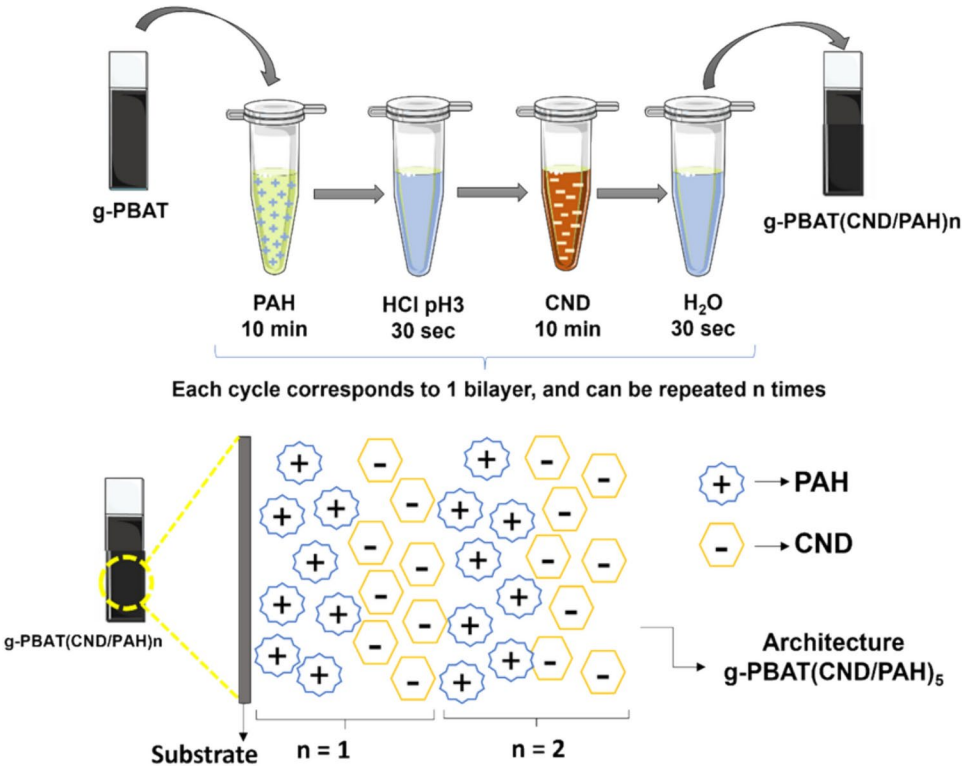

Fig. 1 Scheme of the g-PBAT electrode modification using LbL film

2.6 Electrochemical Measurements

All experiments were carried out using an Autolab PGSTAT30 (Eco Chemie, Utrecht, The Netherlands) galvanostatic/potentiostat, with a three-electrode electrochemical cell comprising a reference Ag/AgCl electrode (3 M KCl), a platinum auxiliary electrode with an area of 1.0 cm^2, and the g-PBAT(CND/PAH)$_5$ LbL film as the working electrode, which was adequately attached on a glass support, thereby insulating one side of the electrode. Electrochemical characterizations were performed in the presence of 5.0 mM $Fe(CN)_6^{-3/-4}$ with 0.1 M KCl as a supporting electrolyte via CV (scan rate of 50 mV s^{-1} over a potential range of − 0.6 V to 0.4 V) and EIS (frequency range of 10^5 Hz to 0.1 Hz with an amplitude of 10 mV). The DPV technique detected analytes over a potential range of − 1.20 to − 0.4 V at a scan rate of 50 mV s^{-1}, in a 0.1 M phosphate buffered saline (PBS) solution. Additionally, different analytes were studied to verify the sensor's selectivity with the individual addition of hydroquinone and methyl parathion (0.50 uM in 0.1 M PBS buffer pH 7.0) as possible interfering species.

2.7 Reprocessing of Sensors After Use

The g-PBAT substrate was produced by mixing 1 g of PBAT with 2.33 g of graphite (ratio 70:30 m/m). After producing the substrate, the electrodes were manually cut. These electrodes were modified using LbL and used in the electrochemical measurements. After use, the electrodes were dried for at least 24 h at room temperature and ground in an IKA® A11 basic analysis mill. The material obtained (3.33 g) was mixed with 10 mL of chloroform to prepare the reprocessed substrate.

3 Results and Discussion

3.1 CND Synthesis

The CNDs are predominantly composed of tri-s-triazine rings. In this context, urea, a nitrogen-rich precursor, was chosen as a bottom-up synthesis approach for the preparation of CND. Additionally, citric acid was incorporated as a second precursor to enhance the presence of carboxylic functional groups on the surface of CNDs [15]. The efficient production of CNDs was confirmed through the fluorescence spectrum analysis, revealing an emission band around 450 nm when excited at 340 nm (Fig. 2A). These results, in line with the literature, indicate control over the surface states or emission centers of the CNDs [15, 16].

Raman spectroscopy is extensively employed to comprehend the evolution of microstructures in carbon-based materials [17]. This is primarily due to its high sensitivity to sp^2 carbon structures, and its capabilities allow for measurements at the nanoscale, rendering it a crucial tool in this investigation [18]. Figure 2B show the replication of the Raman analysis for three distinct points in the CNDs, highlighting the absence of variations in peak patterns and intensity among them. The presence of amorphous or disordered carbon, as evidenced in the CNDs Raman spectrum, resulted in a broad band in the 1000–1500 cm^{-1} range. The synthesis process, particularly the microwave heating step, may contribute to the formation of carbon structures with a lower degree of order. Citric acid exhibits characteristic vibrational modes in this range. Its contributions may be related to carbonyl group (C=O) and hydroxyl group (O–H) bonds. Additionally, one can anticipate observing vibrational modes associated with the C–N and N–H bonds present in urea [19].

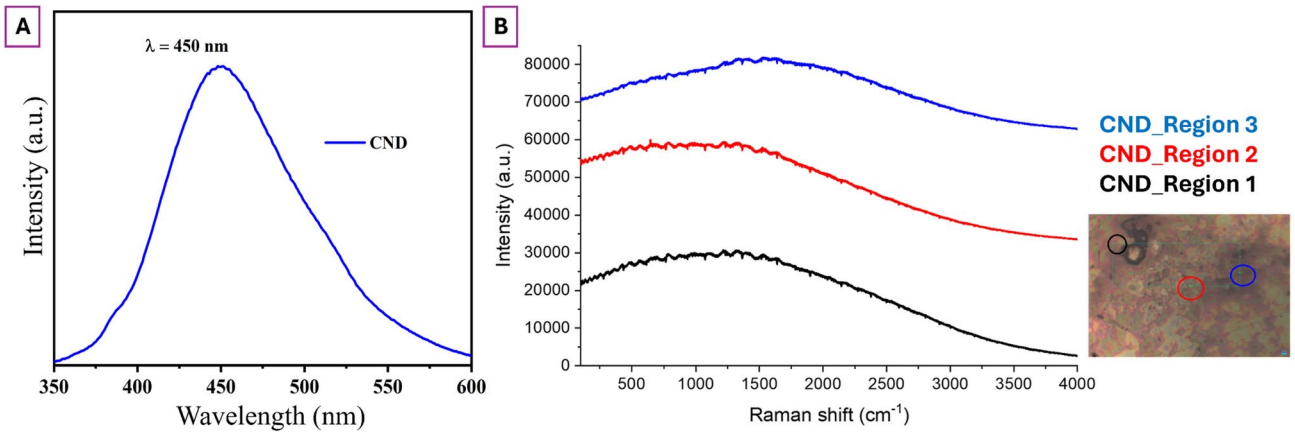

Fig. 2 Emission spectrum for synthesizing CND under an excitation wavelength of 340 nm (**A**), and Raman Spectra of CND in several regions (**B**)

3.2 Study of Bilayer Growth by Layer-by-Layer

The CND and PAH solutions, both at a concentration of 1 mg/mL, used for preparing the LbL films, were previously analyzed by UV–Vis, Fig. 3A. For the PAH sample, no characteristic bands were observed in the range of 190 to 800 nm. In contrast, the CND solution exhibited two bands at 282 nm and 337 nm, the latter of which has been previously described in the literature for CNDs synthesized with urea precursors [15], as in this study. These bands were used as reference points to monitor the deposition of the CND/PAH bilayers, as shown in the inset of Fig. 3B. Linear regression analysis (Fig. 3B) of the absorption intensity at 337 nm for each bilayer indicates a progressive increase in the deposited material, as evidenced by the rising absorption intensity in the target region [20]. The R^2 value of 0.93 demonstrates a linear growth of the bilayers, suggesting a uniform deposition with consistent thickness between layers. Additionally, the electrochemical response in CV measurements for 3, 5, 7, and 9 bilayers influenced the choice of architecture, with the best results observed for 5 bilayers (Fig. SI2).

3.3 Physical Characterizations

To determine whether the wettability of the sensor changed after covering it with the LbL film, contact angle measurements with water were performed. Figure 4 shows the interaction of the drop with the surfaces of g-PBAT (Fig. 4A) and g-PBAT(CND/PAH)$_5$ (Fig. 4B), along with their respective contact angle values. The g-PBAT exhibited a higher contact angle ($94° \pm 1°$), indicating a more hydrophobic nature of the material. After modification with the LbL film, the substrate's wettability increased, becoming more hydrophilic with a contact angle of $80° \pm 1°$. This reduction in contact angle for g-PBAT(CND/PAH)$_5$ was anticipated, as the film was prepared in water and both PAH and CND have hydrophilic properties. This hydrophilicity results from the abundant hydrogen bonding interactions between the hydroxyl groups (-OH) of CND, amine groups (-NH) of PAH polyelectrolytes, and water [21]. The increased hydrophilicity is a desired modification as it enhances interactions between the sensor and the aqueous medium used for electrochemical measurements. This behavior of increased hydrophilicity after coating with LbL film has been previously reported in the literature [3, 5].

The micrograph of the g-PBAT surface (Fig. 4C) revealed a homogeneous dispersion of the filler (graphite) throughout the PBAT matrix, with an ordered aggregation of graphite particles. The surface irregularity led to the formation of conductive areas due to the compaction of the particles. Additionally, the high porosity and small cavities on the sensor surface enhance the number of active sites, as observed in other studies [22, 23]. Conversely, the g-PBAT(CND/PAH)$_5$ films (Fig. 4D) showed no significant morphological changes compared to neat g-PBAT [5]. The deposited (CND/PAH)$_5$ film is indicated by the change in surface color of the sample, with a highlighted area (yellow dotted circle) showing where the film appears to have detached, revealing the substrate with a darker contrast.

FTIR analysis (Fig. 4E) was conducted to identify the characteristic functional groups of the g-PBAT substrate and any chemical modifications resulting from the LbL coating. Although PBAT has several characteristic bands, the incorporated of 70% graphite into the polymer masks some of these bands. For g-PBAT, a band at 1702 cm^{-1} corresponds to the stretching vibration of the ester C=O, and another at 1246 cm^{-1} is related to the bending vibration of the trans-CH_2 plane [24]. Additionally, a C–O band at 1101 cm^{-1}, refers to the absorption of symmetric stretching vibration [25], and a band at 722 cm^{-1} is related to the vibrations of adjacent methylene groups (–CH_2–) [26]. Some

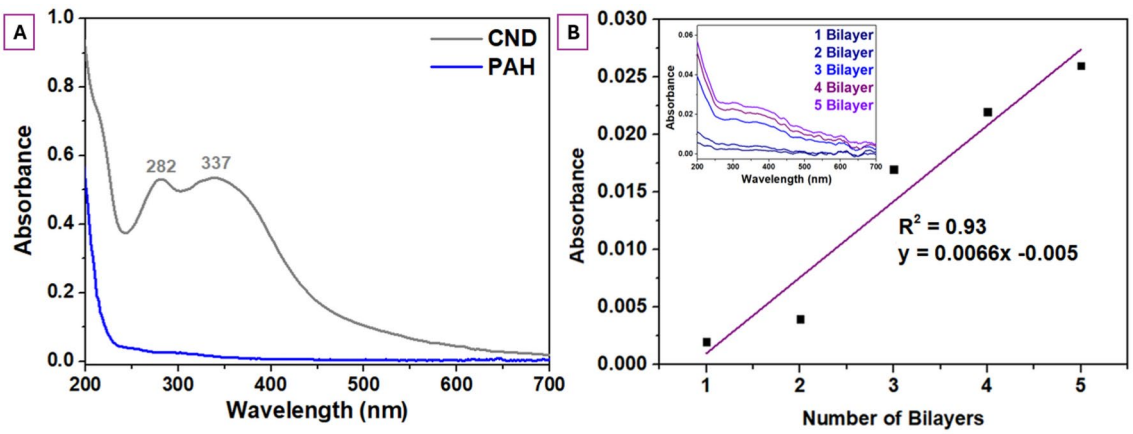

Fig. 3 UV–Vis spectra: **A** CND and PAH solutions with a concentration of 1 mg/mL and **B** growth of LbL films deposited on quartz substrates with 1–5 bilayers of CND/PAH at 337 nm, (inset) UV–Vis spectra on quartz(CND/PAH)$_n$, being n the number of bilayers

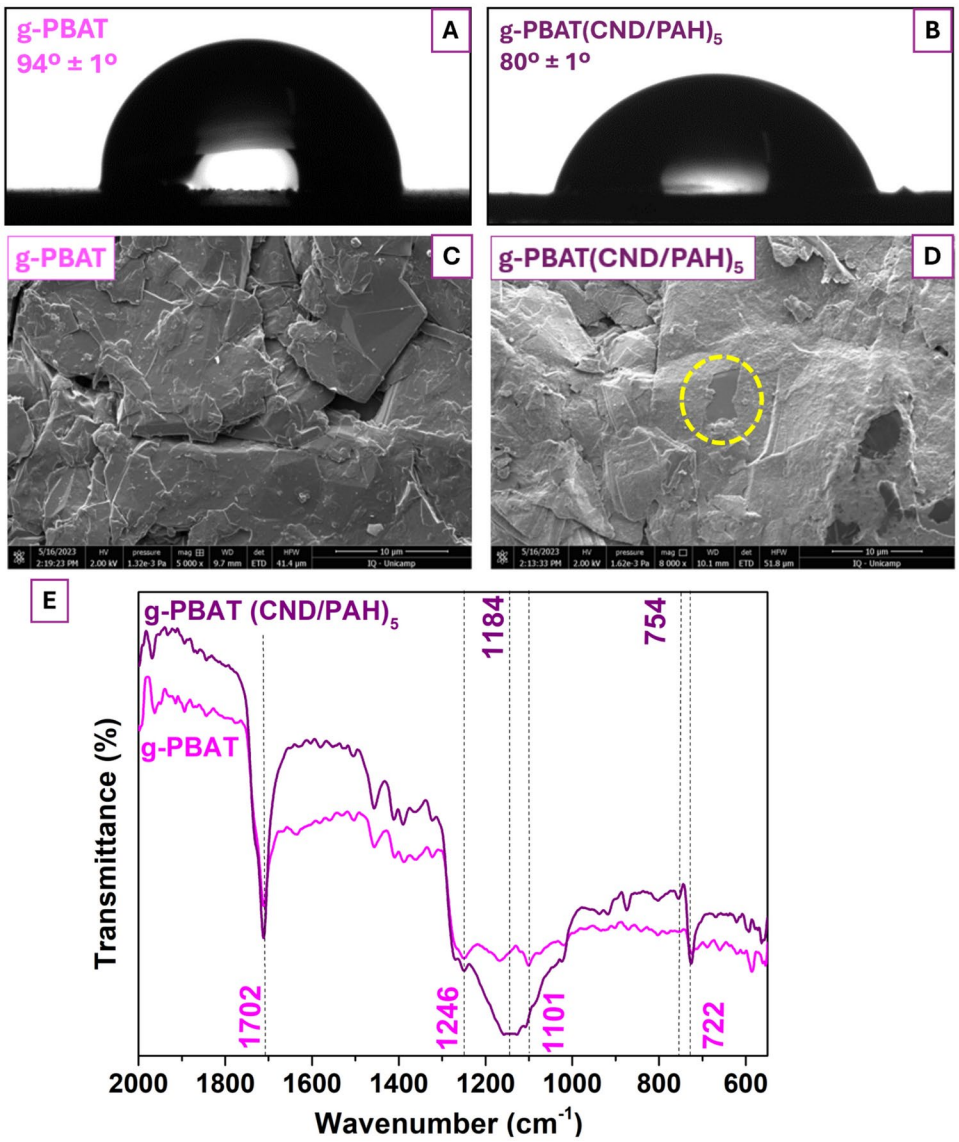

Fig. 4 Surface wettability analyzes of g-PBAT (**A**) and g-PBAT(CND/PAH)$_5$ (**B**). SEM micrographs of the g-PBAT (**C**) and g-PBAT(CND/PAH)$_5$ (**D**) samples, with magnifications of 5000× and 8000×. FTIR spectra of g-PBAT and g-PBAT(CND/PAH)$_5$ (**E**)

modifications were observed for g-PBAT(CND/PAH)$_5$. However, it should be noted that the film's nanometric structure may result in less sensitivity during ATR analysis. Two regions with more evident changes were observed at 1184 and 754 cm^{-1}, attributed to CND. The first band refers to –C–O– and C–OH groups [27], while the second corresponds to carbon nitride rings [15]. Fig. SI1 shows the FTIR spectrum obtained for the CND and the assignments of their main characteristic bands in Table SI1.

In the Raman spectroscopy of graphite materials, the D and G bands are crucial. Specifically, the D band is associated with defects in the sp^3 carbon network, such as edge-plane vibrations, vacancies, and grain boundaries resulting from these imperfections, while the G band correspond to sp^2 planar stretching vibrations [28]. Figure 5A illustrates the Raman spectrum of the g-PBAT electrode, displaying three distinct graphite bands. The band at 1337 cm^{-1} is linked to sp^3 carbons and is influenced by the carbon content in this hybridization. The prominent G band at 1581 cm^{-1} is attributed to sp^2 carbons, and the third band at 2687 cm^{-1}, represents the second-order 2D band [28]. Figure 5B shows that when g-PBAT is used as a substrate for construction the nanostructured film with 5 bilayers of PAH and CND, the characteristic bands of g-PBAT remained evident (Fig. 5A). The only difference observed was that the sample appeared more amorphous with less defined bands, although at the same wavelength.

3.4 Electrochemical Analysis of the Modified Sensor

The CV analysis determines the resulting current of the electrochemical cell, which consists of a working electrode, a platinum counter-electrode, and an Ag/AgCl reference electrode. The resulting voltammogram allows for

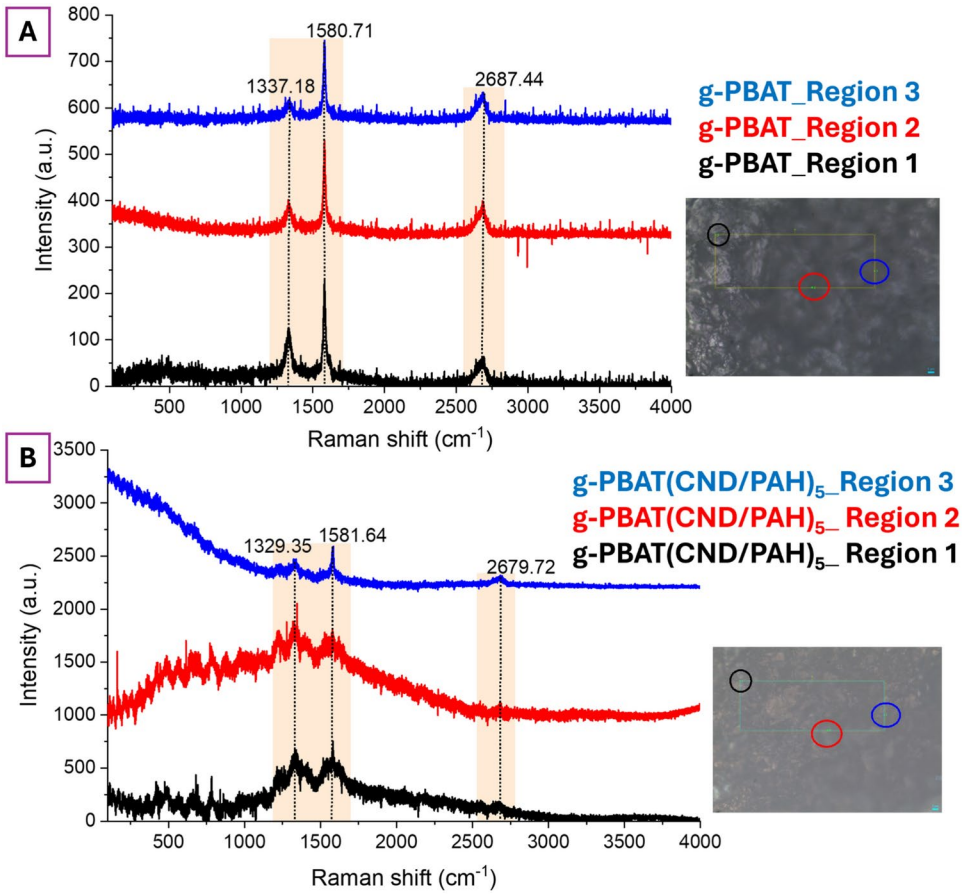

Fig. 5 Raman spectroscopy of the electrode g-PBAT (**A**) and g-PBAT(CND/PAH)$_5$ (**B**)

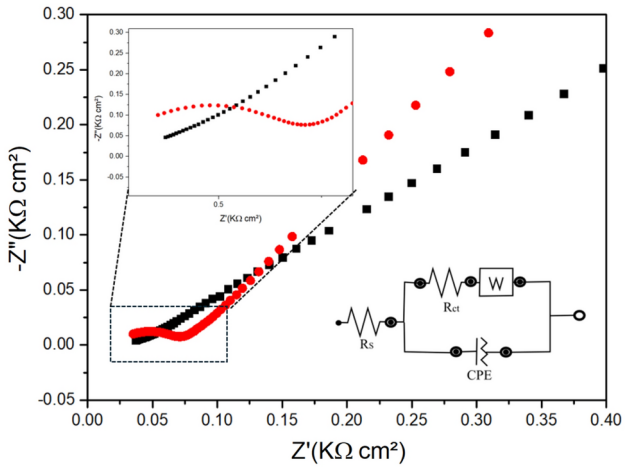

Fig. 6 Electrochemical impedance spectroscopy plot comparing the electrochemical behavior of g-PBAT and g-PBAT(CND/PAH)$_5$. Conditions: medium composed of 5E-3 mol L^{-1} $Fe(CN)_6^{-3/-4}$ with 0.10 mol L^{-1} KCl solution. The applied circuit for electrochemical fitting is also presented, including the Warburg impedance considered for the fitting

the study of the redox behavior of the electrolyte probe solution. Different electrodes exhibit different current responses, and their redox peaks may shift depending on the electrode, which is a critical variable in the analysis. The blank solution indicates whether any electrode material contributes to a redox signal. As mentioned earlier, the probe solution is 5.00 mM $K_3[Fe(CN)_6]$ with 0.10 M KCl. Additionally, EIS was applied to observe the characteristics of the studied electrode compared to the unmodified electrode. This technique provides information about the charge transfer resistance (Rct) by analyzing the equivalent circuit model, as shown in Fig. 6. The Rct and other parameters, such as the electroactive area (A) (cm^2), and the heterogeneous electron transfer constant (k_0), were determined using the Randles–Sevcik (Eq. 1).

$$I_p = \pm \left(2.69E^5\right) n^{3/2}\ A\ D^{1/2}\ C\ v^{1/2} \quad (1)$$

where I_p is the peak current, n is the number of transferred electrons, A is the electroactive area (cm^2), D is the diffusion coefficient of $[Fe(CN)_6]^{-3/4}$ in 0.10 M KCl solution (7.60E-6 cm^2 s^{-1}) [29], C is the concentration of $[Fe(CN)_6]^{-3/4}$ (mol cm^{-3}), and v is the scanning speed (V s^{-1}). As described in the EIS table, the electroactive area of g-PBAT(CND/PAH)$_5$ film was approximately double that of unmodified g-PBAT. Using the A and the Rct values, the electron transfer rate constant (k^0) was calculated using Eq. 2.

Table 1 Electrochemical parameters obtained for LbL electrodes and g-PBAT (pure) in CV and EIS measurements

Parameters				
electrode unit	J (mA cm^{-2})	Rct (KΩ cm^2)	A (cm^2)	k^0 (cm s^{-1})
g-PBAT(CND/PAH)$_5$	0.38 ± 9.79E-2	0.40 ± 2E-2	0.16	7.67E-4
g-PBAT	0.23 ± 5.25E-2	0.07 ± 1E-2	9.92E-2	8.16E-3

The geometric areas were 0.50 cm^2 for all electrodes

$$K^0 = RT/F^2\ A\ C\ Rct \quad (2)$$

where R is the gas constant (8.31 J mol^{-1} K^{-1}), T is the thermodynamic temperature (298 K), F is the Faraday constant (96,485.33 C mol^{-1}), A is the electroactive area (Table 1), and C is the concentration of redox probe (5E-6 mol cm^{-3}). Based on these calculations, the k^0 value for g-PBAT(CND/PAH)$_5$ was significantly higher compared to the neat g-PBAT electrode, indicating improved electrochemical activity.

3.5 Stability, Performance of g-PBAT(CND/PAH)$_5$ Electrode Modified

The reproducibility study (intra-day) of the g-PBAT(CND/PAH)$_5$ electrode was assessed using five electrodes with the probe solution, $K_3[Fe(CN)_6]$, at a concentration of 5 mM, and scan rate of 50 mV s^{-1}. This resulted in a relative standard deviation (RSD) of 14%. For the repeatability test, the sensor was used over six days (inter-day), yielding an RSD of 8.8%, which indicates a slight loss in sensitivity. This sensitivity loss can be attributed to layer damage caused by the electrode's contact with water, the solvent used in the CND solution, and the subsequent immersion in $K_3[Fe(CN)_6]$ solution. The stability of the electrode was evaluated through 50 sequential cycles at a scan rate of 50 mV s^{-1}. After this process, the peak current signal increased by only 8.50% compared to the initial cycle.

3.6 Electrochemical Performance for Detection of PQ and CBF

After establishing the material's behavior with the probe solution, the analysis with the pesticides PQ and CBF was initiated. Detection of these compounds was performed using DPV. This section covers the pH study to identify the optimal pH for the PBS solution, the construction of a standard curve to validate the sensor's performance, and the investigation of potential interferents that might affect detection capabilities.

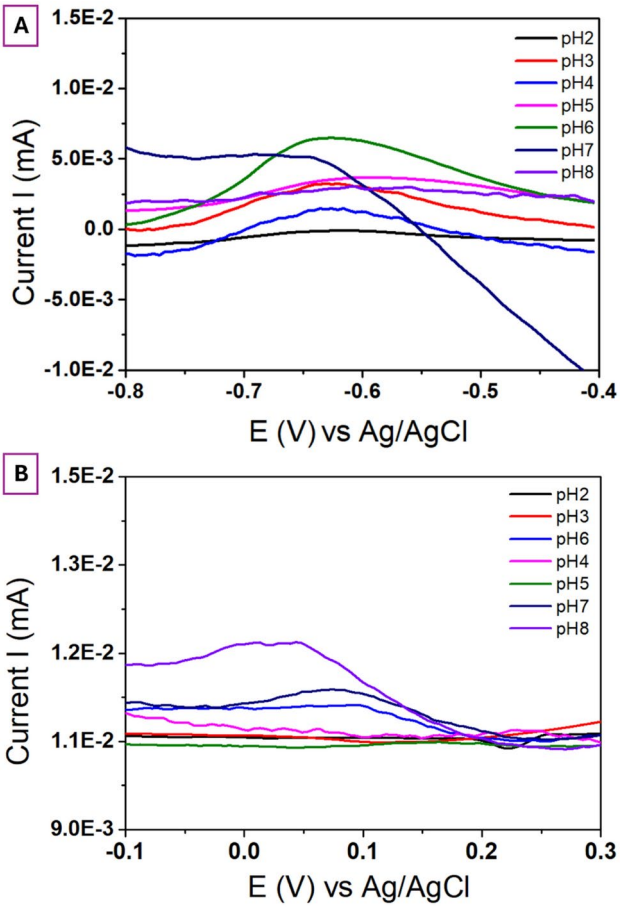

Fig. 7 DPV profiles for PQ at 0.50 µM in the PBS solution, pH (3.0–8.0), using the g-PBAT(CND/PAH)$_5$ electrode. DPV conditions: scan rate 50 mV s^{-1} and potential range from −1.20 V to −0.40 V (**A**). Profiles for CBF at 0.50 mM in the PBS solution. DPV conditions: scan rate 50 mV s^{-1} and potential range from − 0.20 V to 0.40 V (**B**)

3.6.1 pH Study for PQ and CBF Detection

DPV analysis of buffer solutions revealed two reduction peaks for PQ and no oxidation peak. Various pH concentrations were examined to compare peak definitions and establish a standard curve. PBS pH values ranged from 3.0 to 8.0, with g-PBAT(CND/PAH)$_5$ used as the electrode and PQ at a concentration of 0.50 µM. Figure 7 shows the results: acidic buffers (pH 3.0–5.0) displayed no significant peak, only a flat region instead of the expected peak at -0.65 V, as seen in the CV of PQ. The pH concentrations of 6.0 and 7.0, however, showed a peak at the expected region (− 0.65 V), with pH 6.0 providing the most distinct peak. More pronounced peaks facilitate better detection of low concentrations of analytes. The pH 8.0 buffer, like the acidic buffers (pH 3.0–5.0), also showed no peak at the expected potential of − 0.65 V. Similar parameters were used for studying CBF, with results indicating that the pH ranges of 3.0 to 8.0 in acidic buffers (3.0–5.0) showed no significant peak,

displaying a flat region instead of the peak at 0.10 V. In contrast, neutral and slightly alkaline pH solutions exhibited a stronger current at the same potential. Based on these results, pH 7.0 was chosen for analyte detection due to its suitable signal response in PBS.

Regarding the reduction mechanism, previous studies indicate that PQ undergoes a two-electron reduction by capturing electrons from the oxygen present in the solution [30]. The reduction mechanism involves the pyridinium ring receiving an electron from oxygen and being converted to pyridine, as shown in Fig. 8A. Since PQ contains two pyridinium rings, the reduction process occurs twice. The molecule follows a redox cycle mechanism, where an electron can be donated back to the medium, resulting in the oxidation of the nitrogen atom in pyrimidine [31, 32]. CBF, on the other hand, undergoes an oxidation mechanism involving its phenolic ring. This mechanism is well-documented [33] and involves the electrochemical oxidation of the compound, transforming the hydroxyl group on the phenolic ring into a quinone form. This process is illustrated in Fig. 8B.

3.6.2 Calibration Curve to Determine the Concentration of PQ and CBF

Considering the current use of PQ as pesticide in the environment, this study focused on detecting low concentrations. The range considered started at 0.20 µM (0.50 parts per million, ppm) and extended to 5 µg/mL. The standard curve was created based on the pH study, identifying the current peak at − 0.65 V for the interaction between the g-PBAT(CND/PAH)$_5$ electrode and PQ. which found the current peak (− 0.65 V). For CBF, another pesticide, the concentration range was higher due to its limit of quantification (LoQ), varying from 5 µM to 55 µM. The interaction between the g-PBAT(CND/PAH)$_5$ electrode and CBF was observed at a potential of 0.10 V in PBS pH 7.0. Figure 9 shows the peak overlays in different concentrations.

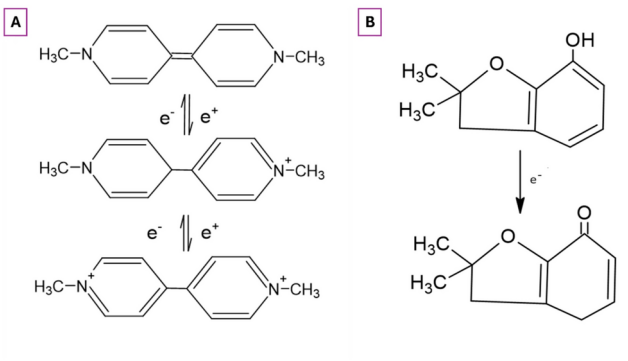

Fig. 8 Reduction of PQ molecule. It shows the redox cycle of PQ which, of the pyridinium ring changes to pyridine during reduction, receiving an electron from an oxygen molecule, and otherwise the oxidation (**A**). Reduction of CBF molecule. It shows the electron-oxidation of a molecule, in which the phenol ring becomes a quinone structure (**B**)

The linear relationship between current and concentration allowed for the development of fitting equati0ons that describe this dependence. Using the York method, Fig. 9A presents the calibration curve equation for PQ, with an adjusted R-squared value of 97.9% and a sensitivity of 3.69E-5 ± 5.94E-7 A cm^{-2} M^{-1}. Figure 9B presents the calibration curve equation for CBF, with an adjusted R-squared of 94.1% and sensibility of 2.51E-7 ± 2.09E-8 A cm^{-2} M^{-1}.

As previously discussed, the peak with the highest signal, at − 0.65 V, was used as a reference for the structure. Based on the calibration curve and the DPV curves of blank solutions, the LoD and LoQ were calculated according to IUPAC recommendations. Studying these limits is crucial to accurately reflect the true analytical signal, considering the current density indicated by blank analyses. This directly affects the results from real samples due to material and surface modifications, as described in Eqs. 3 and 4.

$$\mathrm{LoD} = (\mathrm{yD} - \bar{\mathrm{y}}\mathrm{B})/\mathrm{q1} = \mathrm{kD}\sigma\mathrm{b}/\mathrm{q1} \tag{3}$$

$$\mathrm{LoQ} = (\mathrm{yQ} - \bar{\mathrm{y}}\mathrm{B})/\mathrm{q1} = \mathrm{kQ}\sigma\mathrm{b}/\mathrm{q1} \tag{4}$$

The values of these limits were determined by combining the data obtained from the calibration curve and the blank solution. The mean blank signal is represented by $\bar{y}B$, and σb denotes the relative standard deviation of the blank solution. The LoD and LoQ are denoted by yD and yQ, respectively. These values account for blank correction and are replaced by kD (corresponding to 3) and kQ (corresponding to 10). The slope of the calibration curve is represented by q1 [34]. The LoD values for PQ and CBF were found to be 0.63 and 7.14 µM, respectively. This indicates the lowest concentrations that the g-PBAT(CND/PAH)5 electrode can detect, while the LoQ values are 2.10 and 23.80 µM, representing the lowest concentrations that can be reliably quantified, considering reproducibility and accuracy.

The LoD values are like those found in other studies and sensors. Table 2 summarizes various substrates with surface modification sensors for PQ and CBF, including their LoD features. When compared to other electrodes, the LoD values for PQ and CBF are higher for nearly all electrodes listed. This is expected, given that this electrode can simultaneously detect two analytes, particularly for CBF, which shows a difference of over 700 times compared to the Gd_2S_3/RGO/GCE electrode. Nonetheless, the g-PBAT(CND/PAH)$_5$ electrode still detects concentrations in the µM range.

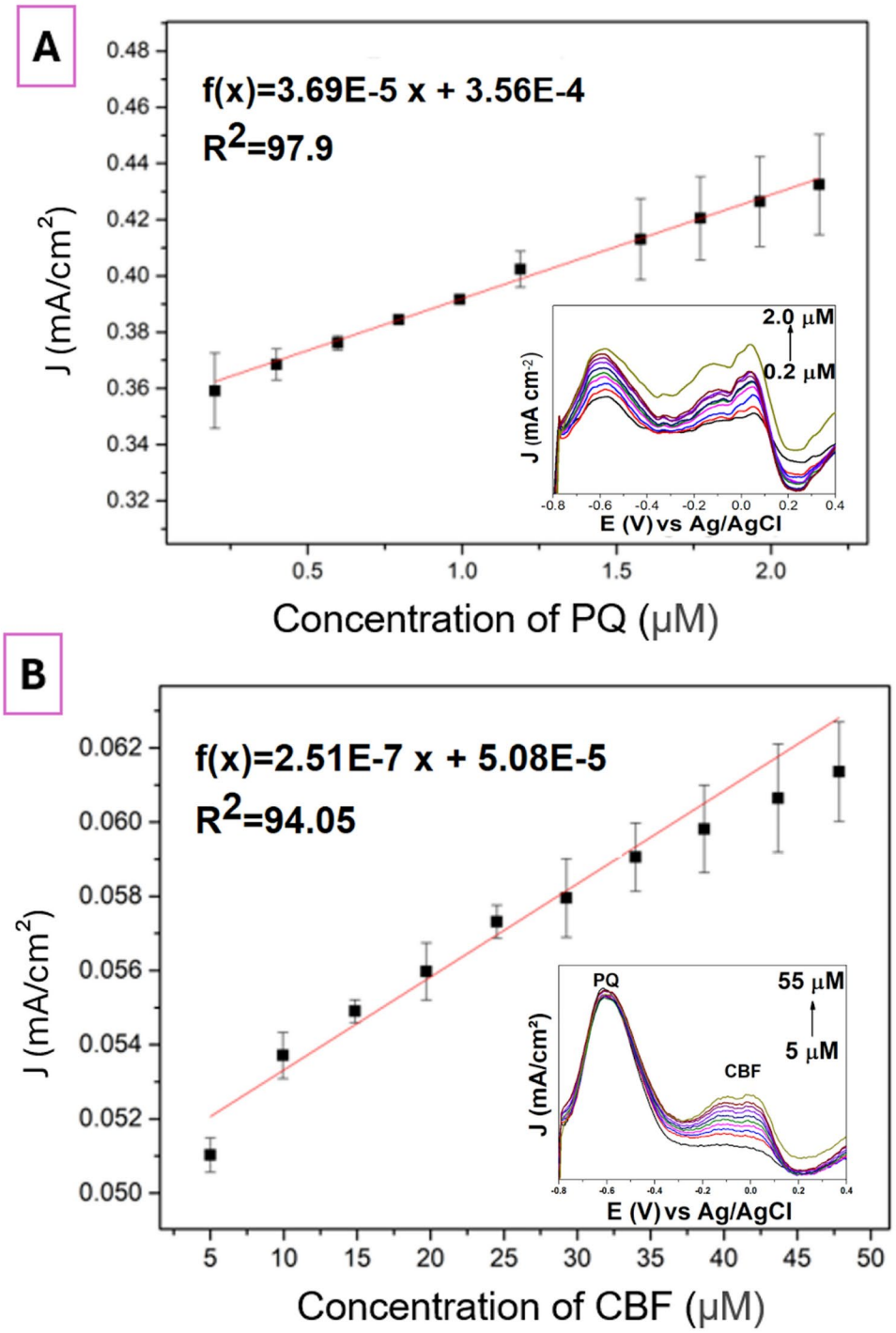

Fig. 9 Standard curve of electrochemical response for PQ sensor obtained with DPV in 0.10 M PBS (pH 7.0) using g-PBAT(CND/PAH)$_5$ electrode with a concentration ranging from 0.20 to 2 µM (**A**). Standard curve of electrochemical response for CBF sensor obtained with DPV in 0.1 M PBS (pH 7.0) using g-PBAT(CND/PAH)$_5$ electrode with a concentration ranging from 5 to 55 µM (**B**)

3.6.3 Analysis of Real Water Samples and Interfering Species

The g-PBAT(CND/PAH)$_5$ sensor was evaluated using an addition–recovery methodology. Known quantities of PQ and CBF were spiked into tap water samples and then diluted in PBS at pH 7.0. Two different concentrations of each compound were analyzed in triplicate using DPV under optimized conditions. Table 3 presents the actual concentration values, the concentrations determined from the calibration curve, and the recovery values for the tap water samples. For PQ, the recoveries with the g-PBAT(CND/PAH)$_5$ sensor ranged from 89.3% to 105% of the theoretical values, while for CBF, the recoveries ranged from 92.1% to 105.9% of the theoretical values. These results indicate that the proposed sensor exhibits good sensitivity for real

Table 2 Comparing other surface modified sensors' limit of detection for PQ and CBF in the literature to the one proposed, the description of each is presented in the Table S2 in support information file

Working electrode	Sample	Concentration range (µM)	LoD (µM)	References
g-PBAT(CND/PAH)$_5$	PQ	0.20–2.00	0.63	This work
	CBF	5.00–55.00	7.14	
PPY-g-NGE/GCE	PQ	0.05–2.00	0.04	[35]
AuNPs/DNA/GE	PQ	0.00–100.00	1.30	[36]
MWCNTs-DHP/CG	PQ	0.05–1.60	0.01	[37]
g-PBAT(PPY/CNT)$_7$	PQ	0.10–2.10	0.07	[5]
nano-MIL-101(Cr)/GC	CBF	1.00–20.00	0.96	[38]
Gd_2S_3/RGO/GCE	CBF	0.01E-1–138.00	0.01	[33]
C/VO@GCE	CBF	0.05–75.00	0.06	[8]

Table 3 Comparison of concentration applied in the electrode to the recovered signal of current density applied in the calibration curve

Compound	Concentration applied (µM)	Mean concentration recovered (µM)	RSD
PQ	0.70	0.65 ± 0.06	6.26%
PQ	1.40	1.43 ± 0.06	4.08%
CBF	20.00	20.46 ± 1.47	7.56%
CBF	43.00	43.79 ± 1.98	4.52%

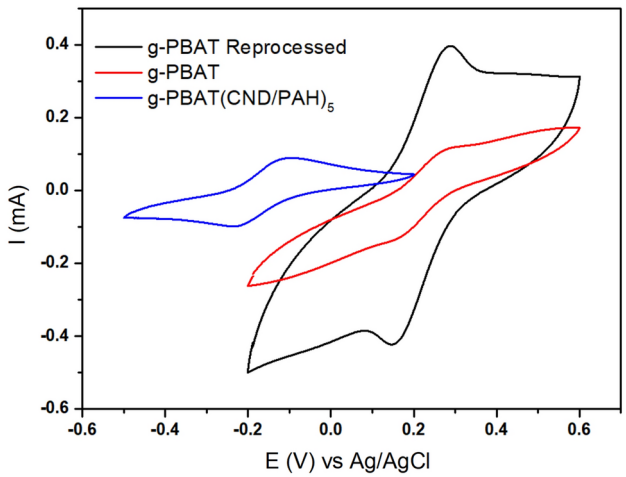

Fig. 10 The CV results for the three types of electrodes, g-PBAT reprocessed (black line), g-PBAT (red line) and g-PBAT(CND/PAH)$_5$ (blue line). Conditions: CV was used over a potential range of − 0.20 V to + 0.60 V (g-PBAT and g-PBAT reprocessed) and − 0.50 V to + 0.20 V (g-PBAT(CND/PAH)$_5$) with a scan rate of 50 mV s^{-1}. All measurements were performed in 5E-3 M $K_3[Fe(CN)^6]$ with 0.10 M KCl solution as a supporting electrolyte

sample applications and routine pesticide analysis, with a stable relative standard deviation (RSD) ranging from 4.0% to 7.5% [5]. The interfering species studied were methyl parathion (PR) and hydroquinone (HQ) at a concentration of 0.50 µM. The results (Fig. SI3) showed that these compounds did not interfere with the detection of PQ and CBF, with the test statistic (test-T < 5%). This demonstrates that the g-PBAT(CND/PAH)$_5$ electrode has good selectivity for PQ and CBF detection, showing no interference from commonly coexisting substances.

3.7 Reprocessed Electrode

Most electrodes used in research are disposable, which presents an environmental issue. Although these electrodes are made from biodegradable polymers designed to detect pesticide pollutants and protect the environment, they need to be reintegrated into a sustainable cycle. This work focuses on reprocessing used electrodes to make them suitable for reuse.

3.7.1 Electrochemical Characterization

After the process described in Sect. 2.7, the retrieved electrodes were compared to new electrodes made of g-PBAT and the LbL-modified electrode, g-PBAT(CND/PAH)$_5$, using CV analysis. The parameters for analysis were the same as previously described, with a probe solution of 5 mM $K_3[Fe(CN)_6]$ in 0.10 M KCl and a scan rate of 50 mV s^{-1}. Figure 10 shows the CV results for the three types of electrodes. It is evident that there is a notable difference between the g-PBAT and g-PBAT(CND/PAH)$_5$ electrodes, attributed to the LbL modification, which alters the electroactive surface and causes a shift in the redox peaks [39]. The reprocessing removed the LbL surface treatment, resulting in a shift in the potentials relative to the original g-PBAT redox peaks. Although the reprocessed g-PBAT and the new g-PBAT electrodes exhibited similar potentials, they showed different currents. This discrepancy is due to the inability to accurately define the electroactive area for current density analysis. While the reprocessing shows promise, further analysis is needed to validate its effectiveness for reuse.

4 Conclusion

The developed substrate (g-PBAT) was successfully modified with the LbL nanostructured film (g-PBAT(CND/PAH)$_5$) using the LbL technique. The growth of the bilayers was monitored by UV–Vis spectroscopy, showing a progressively self-assembled structure with homogeneous layers. Both functionalized and non-functionalized substrates were characterized, and the results highlighted the modifications introduced by the LbL film. Following functionalization, the electrode exhibited increased hydrophilicity, which is advantageous for applications in aqueous environments where electrochemical measurements were conducted. Microscopic analyses revealed a porous and irregular surface with an enhanced electroactive area. Infrared and Raman spectroscopy also indicated changes due to the film's presence. The electrochemical characterization demonstrated good reproducibility, repeatability, and stability, with an increased current signal peak compared to the initial cycle. The modified sensor displayed excellent selectivity for detecting PQ and CBF, even in the presence of potential interfering species. The reprocessing study yielded promising results, as the electrochemical response of reprocessed material showed redox peaks similar to those of the initial g-PBAT. Additionally, physical fragmentation combined with chemical solubilization in chloroform effectively disassembled the LbL-modified films, resulting in shifts of peaks for functionalized samples.

Supplementary Information The online version contains supplementary material available at https://doi.org/10.1007/s11244-024-02014-7.

Acknowledgements This work was funded by São Paulo State Research Support Foundation (FAPESP)—2023/06505 (MF), 2023/17363-0 (ASMF) and 2023/00335-4 (JSR); Coordination for the Improvement of Higher Education Personnel (CAPES)—88887.803614/2023-00 (LVBVF); National Council for Scientific and Technological Development (CNPq)—169054/2023-3 (SFA) and 381705/2024-2 (MESN). The authors would like to thank the Servier Medical Art image bank and our collaborator Jefferson Israel da Silva.

Data availability The data will be available in the UFSCar data repository (https://repositorio.ufscar.br/discover?filtertype=type&filter_relational_operator=equals&filter=Dataset). After publication, the data repository will be fed with the final data generated in the research. They will be made available in Origin or Excel spreadsheet forms. Each set of files will be assigned a name and a data item. Thus, the data will be open and preserved in all details.

Declarations

Conflict of interest The authors declare that they have no known competing financial interests or personal relationships that could have appeared to influence the work reported in this paper.

References

1. Sinha E, Calvin KV, Kyle PG et al (2022) Implication of imposing fertilizer limitations on energy, agriculture, and land systems. J Environ Manage 305:114391. https://doi.org/10.1016/j.jenvman.2021.114391
2. Wong A, Santos AM, da Fonseca AR et al (2021) Simultaneous determination of direct yellow. Talanta. https://doi.org/10.1016/j.talanta.2020.121539
3. Maciel CC, de Freitas ASM, Medrades JP, Ferreira M (2022) Simultaneous determination of catechol and Paraquat using a flexible electrode of PBAT and graphite modified with gold nanoparticles and copper phthalocyanine (g-PBAT/AuNP/CuTsPc) LbL film. J Electrochem Soc 169:027505. https://doi.org/10.1149/1945-7111/ac4ff0
4. Sukanya, Kumara Swamy BE, Shashikumara JK (2020) Poly (benzydamine) sensor for electrochemical resolution of catechol and hydroquinone. Mater Sci Energy Technol 3:640–647. https://doi.org/10.1016/j.mset.2020.06.009
5. Amaro SF, Maciel CC, Rodrigues JS et al (2023) Investigation of the synergistic effect of layer-by-layer films of carbon nanotubes and polypyrrole on a flexible electrochemical device for Paraquat sensing. Chemosensors. https://doi.org/10.3390/chemosensors11080420
6. Wang CH, Zhang XW, Chen DT et al (2024) Utilizing symmetrical tetramethyl cucurbit[6]uril-based supramolecular fluorescence probe for detection of paraquat in water. Spectrochim Acta A Mol Biomol Spectrosc. https://doi.org/10.1016/j.saa.2024.123845
7. Kempuraj D, Zhang E, Gupta S et al (2023) Carbofuran pesticide toxicity to the eye. Exp Eye Res. https://doi.org/10.1016/j.exer.2022.109355
8. Prashanth MK, Shanavaz H, Yogesh Kumar K et al (2024) Facile synthesis of limeonia acidissima shell derived carbon-vanadium pentoxide nanocomposite for sensitive detection of carbofuran. Results Chem 2024:2211–7156. https://doi.org/10.1016/j.rechem.2024.101401
9. Kongkaew S, Kanatharana P, Thavarungkul P, Limbut W (2021) Studying the preparation, electrochemical performance testing, comparison and application of a cost-effective flexible graphene working electrode. J Colloid Interface Sci 583:487–498. https://doi.org/10.1016/j.jcis.2020.08.121
10. Mccord CP, Ozer T, Henry CS (2021) Synthesis and grafting of diazonium tosylates for thermoplastic electrode immunosensors HHS public access. Anal Methods 13:5056–5064. https://doi.org/10.1039/x0xx00000x
11. de Freitas ASM, Maciel CC, Lemes AP, Ferreira M (2022) Thermoplastic starch and graphite biocomposite electrode for electrochemical catechol sensor. ECS Adv 1:036504. https://doi.org/10.1149/2754-2734/ac936d
12. De Lima LF, De A, De Freitas SM et al (2022) Enzymeless glucose sensor based on disposable Ecoflex®/graphite thermoplastic composite substrate modified with Au@GQDs. Sens Actuators Rep 4:100102. https://doi.org/10.1016/j.snr.2022.100102
13. Koel M (2024) Developments in analytical chemistry initiated from green chemistry. Sustain Chem Environ 5:100078. https://doi.org/10.1016/J.SCENV.2024.100078
14. Zhang X, Xu Y, Zhang X et al (2019) Progress on the layer-by-layer assembly of multilayered polymer composites: strategy, structural control and applications. Prog Polym Sci 89:76–107. https://doi.org/10.1016/j.progpolymsci.2018.10.002
15. Liyanage PY, Graham RM, Pandey RR et al (2019) Carbon nitride dots: a selective bioimaging nanomaterial. Bioconjug Chem 30:111–123. https://doi.org/10.1021/ACS.BIOCONJCHEM.8B00784

16. Maciel CC, De Barros A, Mazali IO, Ferreira M (2023) Flexible biodegradable electrochemical sensor of PBAT and CNDs composite for the detection of emerging pollutants. J Electroanal Chem. https://doi.org/10.1016/j.jelechem.2023.117491
17. Guizani C, Haddad K, Limousy L, Jeguirim M (2017) New insights on the structural evolution of biomass char upon pyrolysis as revealed by the Raman spectroscopy and elemental analysis. Carbon NY 119:519–521
18. Smith MW, Dallmeyer I, Johnson TJ et al (2016) Structural analysis of char by Raman spectroscopy: improving band assignments through computational calculations from first principles. Carbon. https://doi.org/10.1016/j.carbon.2016.01.031
19. Zhang Y, Pan Q, Chai G et al (2013) Synthesis and luminescence mechanism of multicolor-emitting g-C_3N_4 nanopowders by low temperature thermal condensation of melamine. Sci Rep. https://doi.org/10.1038/srep01943
20. Mercante LA, Scagion VP, Pavinatto A et al (2015) Electronic tongue based on nanostructured hybrid films of gold nanoparticles and phthalocyanines for milk analysis. J Nanomater. https://doi.org/10.1155/2015/890637
21. De Lima LF, Maciel CC, Ferreira AL et al (2018) An investigation of the synergistic effect between magnetite nanoparticles and polypyrrole in nanostructured layer-by-layer films. J Appl Polym Sci. https://doi.org/10.1002/app.49750
22. Klunder KJ, Nilsson Z, Sambur JB, Henry CS (2017) Patternable solvent-processed thermoplastic graphite electrodes. J Am Chem Soc. https://doi.org/10.1021/jacs.7b06173
23. Perween M, Parmar DB, Bhadu GR, Srivastava DN (2014) Polymer–graphite composite: a versatile use and throw plastic chip electrode. Analyst 139:5919–5926. https://doi.org/10.1039/c4an01405g
24. Nagarajan V, Misra M, Mohanty AK (2013) New engineered biocomposites from poly(3-hydroxybutyrate-co-3-hydroxyvalerate) (PHBV)/poly(butylene adipate-co-terephthalate) (PBAT) blends and switchgrass: fabrication and performance evaluation. Ind Crops Prod 42:461–468. https://doi.org/10.1016/j.indcrop.2012.05.042
25. Nobile MR, Crocitti A, Malinconico M et al (2018) Preparation and characterization of polybutylene succinate (PBS) and polybutylene adipate-terephthalate (PBAT) biodegradable blends. AIP Conf Proc 1981. https://doi.org/10.1063/1.5046042/1027010
26. Sangroniz A, Sangroniz L, Aranburu N et al (2018) Blends of biodegradable poly(butylene adipate-co-terephthalate) with poly(hydroxi amino ether) for packaging applications: miscibility, rheology and transport properties. Eur Polym J 105:348–358. https://doi.org/10.1016/j.eurpolymj.2018.06.016
27. Siddique AB, Pramanick AK, Chatterjee S, Ray M (2018) Amorphous carbon dots and their remarkable ability to detect 2,4,6-trinitrophenol OPEN. Sci Rep. https://doi.org/10.1038/s41598-018-28021-9
28. Kim T, Lee J, Lee K-H (2016) Full graphitization of amorphous carbon by microwave heating. RSC Adv. https://doi.org/10.1039/c6ra01989g
29. Sundfors F, Bobacka J, Ivaska A, Lewenstam A (2002) Kinetics of electron transfer between Fe(CN)63−/4− and poly(3,4-ethylenedioxythiophene) studied by electrochemical impedance spectroscopy. Electrochim Acta 47:2245–2251. https://doi.org/10.1016/S0013-4686(02)00063-4
30. Bus JS, Gibson JE (1984) Paraquat: model for oxidant-initiated toxicity. Environ Health Perspect 55:37–46. https://doi.org/10.1289/EHP.845537
31. Rössler SL, Jelier BJ, Magnier E et al (2020) Pyridinium salts as redox-active functional group transfer reagents. Angew Chem Int Ed 59:9264–9280. https://doi.org/10.1002/ANIE.201911660
32. Ledwith A (1977) Biochemical mechanisms of paraquat toxicity. In: Autor AP (ed) Biochemical mechanisms of Paraquat toxicity. American Press, Lake Charles, pp 21–38
33. Mariyappan V, Keerthi M, Chen SM (2021) Highly selective electrochemical sensor based on Gadolinium Sulfide rod-embedded RGO for the sensing of carbofuran. J Agric Food Chem 69:2679–2688. https://doi.org/10.1021/acs.jafc.0c07522
34. Mocak J, Bond AM, Mitchell S, Scollary G (1997) A statistical overview of standard (IUPAC and ACS) and new procedures for determining the limits of detection and quantification: application to voltammetric and stripping techniques. Pure Appl Chem 69:297–328. https://doi.org/10.1351/PAC199769020297
35. Kavazoi HS, Martin CS, Alessio P (2022) Comparative study of tetrasulfonated phthalocyanine modified screen-printed electrodes in paraquat. Synth Met 284:116988. https://doi.org/10.1016/J.SYNTHMET.2021.116988
36. Ribeiro JA, Carreira CA, Lee HJ et al (2010) Voltammetric determination of paraquat at DNA–gold nanoparticle composite electrodes. Electrochim Acta 55:7892–7896. https://doi.org/10.1016/J.ELECTACTA.2010.03.058
37. Garcia LLC, Figueiredo-Filho LCS, Oliveira GG et al (2013) Square-wave voltammetric determination of paraquat using a glassy carbon electrode modified with multiwalled carbon nanotubes within a dihexadecylhydrogenphosphate (DHP) film. Sens Actuators B Chem 181:306–311. https://doi.org/10.1016/J.SNB.2013.01.091
38. Pınar PT, Yardım Y, Gülcan M, Şentürk Z (2023) The first approach for the simultaneous quantification of isoproturon, carbendazim, and carbofuran at the surface of a MIL-101(Cr) metal–organic framework-based electrode. Inorg Chem Commun 156:111327. https://doi.org/10.1016/J.INOCHE.2023.111327
39. Medhin Ashebo M, Liu N, Yu F, Ma J (2024) Surface functional modification of Nb2CTx MXene for high performance capacitive deionization. Sep Purif Technol. https://doi.org/10.1016/j.seppur.2024.127125